



Role of Eddy Diffusion in the Delayed Ionospheric Response to Solar Flux Changes

Rajesh Vaishnav¹, Christoph Jacobi¹, Jens Berdermann², Mihail Codrescu³, and Erik Schmölder²

¹Leipzig Institute for Meteorology, Universität Leipzig, Stephanstr. 3, 04103 Leipzig, Germany

²German Aerospace Center, Kalkhorstweg 53, 17235 Neustrelitz, Germany

³Space Weather Prediction Centre, National Oceanic and Atmospheric Administration, Boulder, Colorado, USA

Correspondence: Rajesh Vaishnav (rajesh_ishwardas.vaishnav@uni-leipzig.de)

Abstract. Simulations of the ionospheric response to solar flux changes driven by the twenty-seven days solar rotation have been performed using the global 3-D Coupled Thermosphere/Ionosphere Plasmasphere electrodynamics (CTIPE) physics-based numerical model. Using the F10.7 index as a proxy for solar EUV variations in the model, the ionospheric delay at the solar rotation period is well reproduced and amounts to about 1 day, which is consistent with satellite and in-situ measurements.

5 From mechanistic CTIPE studies with reduced and increased eddy diffusion, we conclude that the eddy diffusion is a primary factor that influences the delay of the ionospheric total electron content (TEC). We observed the peak response time of atomic oxygen to the molecular nitrogen ratio to solar EUV flux changes quickly during the increased eddy diffusion compared with weaker eddy diffusion. These results suggest that an increase in the eddy diffusion leads to faster transport processes and an increased loss rates resulting in a decrease of the ionospheric time delay. Furthermore, we found that an increase in solar
10 activity leads to an enhanced ionospheric delay. At low latitudes, the influence of solar activity is stronger, as EUV radiation drives ionization processes that lead to composition changes. Hence, the combined effect of eddy diffusion and solar activity lead to longer delay in the low and mid latitude region.

1 Introduction

The solar activity plays a significant role in controlling the variations in the thermosphere/ionosphere (T/I) system, in particular
15 through solar Extreme Ultraviolet (EUV) and Ultraviolet (UV) radiation and their variability. In addition, there are several factors which control the behaviour of the T/I system, like tidal and gravity wave forcing from the lower atmosphere, neutral winds, and related currents in the ionosphere. These are especially predominant during low solar activity, leading to reduced correlation of solar flux and ionospheric electron density then (Vaishnav et al., 2019). The ionosphere itself is created through photoionization of major constituents (atomic oxygen, molecular nitrogen, and molecular oxygen), while photodissociation
20 may change the mixing ratios of these constituents (especially atomic oxygen) and leads to modifications of ionisation rates.

Due to these varying ionization rates for different atoms and molecules, a series of layers of electron density forms, known as D, E, F1, and F2 regions. The maximum peak of electron density is observed in the F2 region. The F2 region electron densities mainly depend on photo-chemical processes such as photodissociation, photoionization and loss through recombination with molecular nitrogen, and transport processes such as neutral wind and diffusion. On top of this, there are many processes



25 which can drive or disturb the ionospheric ion distribution, such as diffusion, transport, cooling, and heating mechanisms. The transport can be divided in three main categories, namely eddy diffusion, molecular diffusion and advection processes (Brasseur and Solomon, 2006). The F2 region is highly influence by the global thermospheric circulation (Rishbeth, 1998).

The physical mechanism of the delayed ionospheric response that cannot be explained with solar variations, seasonal variations or changes due to geomagnetic activity. We also cannot explain the delay with photoionization and photo-dissociation processes alone. This has been discussed in different studies (Jakowski et al., 1991; Schmölder et al., 2018, 2020, & references therein) and the importance of the T/I coupling was pointed out there. The T/I coupling is important for the delay. This has been mentioned in several studies by now but was scarcely investigated. The most important impacts we would expect due to this coupling are composition changes that can impact the major processes and this could be due to gravity waves induced diffusion, etc.

35 The lower thermospheric composition is not only influenced by gravity waves, but also by other parts of the lower atmospheric wave spectrum including atmospheric tides and planetary waves. The main source of eddy diffusion is breaking of gravity waves. Gravity waves are usually generated in the lower atmosphere by different mechanisms such as convection, wind shears, storms, and airflow over mountains. Their amplification and wave breaking due to instabilities produces mixing (Li et al., 2005). Atmospheric tidal and planetary wave activity can also significantly contribute to eddy diffusion. For example, the tides induce a net transport of atomic oxygen via the mean meridional circulation generated by tidal dissipation (Jones et al., 2014a, b). Above the mesopause, the intradiurnal variability associated with atmospheric tides strongly affects the transport of NO_x (Meraner and Schmidt, 2016), and seasonally varying gravity wave and tidal mixing influence in the mesosphere-lower thermosphere (MLT) region (Qian et al., 2013). Moreover, the possible role in the semiannual oscillation in thermospheric mass density is discussed by Jones et al. (2018). Siskind et al. (2014) showed that the vertical transport from nonmigrating tides causes a significant reduction in the calculated peak electron density of the ionospheric F2 layer.

Various studies have reported about the influence of gravity waves and turbulence on the T/I composition and calculated the eddy diffusion coefficient in the MLT region (Kirchhoff and Clemesha, 1983; Sasi and Vijayan, 2001; Swenson et al., 2019). Based on radar measurements, Kirchhoff and Clemesha (1983) calculated a minimum (maximum) eddy diffusion coefficient of 45 (123) $m^2 s^{-1}$ during fall (summer). Similarly, Sasi and Vijayan (2001) used Doppler radar observations and show that the eddy diffusion varies from 25 to 300 $m^2 s^{-1}$ during September and June.

Turbulent mixing is an important process which affects the composition of the T/I system. The effect of turbulence on different minor and major species has been discussed on several occasions (e.g., Keneshea and Zimmerman, 1970; Shimazaki, 1971; Chandra and Sinha, 1974; Rishbeth et al., 1987; Rees and Fuller-Rowell, 1988; Fuller-Rowell and Rees, 1992; Danilov and Konstantinova, 2014; Pilinski and Crowley, 2015; Swenson et al., 2018). Various coupled models have been developed to understand the T/I region variations considering the availability of experimental and theoretical knowledge. Earlier 1-D models, which include eddy diffusion coefficients have been used to model the T/I region (e.g., Colegrove et al., 1965; Shimazaki, 1971; Jakowski et al., 1991). Nowadays, more improved, 3-D models like the Coupled Thermosphere Ionosphere Plasmasphere Electrodynamics (CTIPe) model (Fuller-Rowell and Rees, 1980) or the National Center for Atmospheric Research (NCAR) Thermosphere-Ionosphere-Electrodynamics General Circulation Model (TIE-GCM) (Richmond et al., 1992) are available to



60 explore the dynamics of the T/I region. These models cannot be expected to exactly reproduce the real ionospheric variability due to limited knowledge of various processes in the T/I region and their corresponding inputs (e.g., Shim et al., 2011; Codrescu et al., 2012), but they are able to provide insight into relevant dynamical processes in the T/I.

Rees and Fuller-Rowell (1988) used a sinusoidal eddy turbulence profile and analysed the effect of eddy turbulence on temperature, atomic oxygen, and nitric oxide. They showed that an increase in turbulence near the mesopause leads to an
65 enhancement of atomic oxygen and nitric oxide. This results in a change in thermal structure by strong modification of the gravity wave flux.

The solar radiation reaching the Earth exhibits a periodicity of about 27 d owing to the solar rotation. As a result, the T/I system also varies with this periodicity. Many studies revealed a delay in ionospheric parameters such as total electron content (TEC, given in TEC units, $1 \text{ TECU} = 10^{16} \text{ electrons } m^{-2}$), electron density, peak electron density of the F_2 region
70 (NmF_2, cm^{-3}) and corresponding height (hmF_2, km), to the 27 d solar flux variation (Jakowski et al., 1991; Liu et al., 2006; Afraimovich et al., 2008; Lee et al., 2012; Anderson and Hawkins, 2016; Jacobi et al., 2016; Schmölter et al., 2018, 2020; Vaishnav et al., 2018; Ren et al., 2018, & references therein). Most of the studies found an ionospheric delay of about 1-2 d, with a possible uncertainty of about half a day. Schmölter et al. (2018), using data with high temporal resolution, found an ionospheric delay of about 17-19 h using TEC and Geostationary Operational Environmental Satellites (GOES) EUV datasets.
75 The detailed seasonal and spatial effect on the ionospheric delay was studied by Schmölter et al. (2020). Their study reveals a strong geomagnetic effects on the ionospheric delay. They also noticed that the delay over Southern Hemispheric stations is larger than over Northern Hemisphere stations.

Numerical simulations using a 1-D model have revealed that the delay might be due to slow diffusion of atomic oxygen at 180 km height, generated by solar UV radiation in the Schumann-Runge continuum, which causes photodissociation of
80 molecular oxygen above the turbopause (Jakowski et al., 1991).

Ren et al. (2018) studied ionospheric time delay using observations and simulations with the TIE-GCM. They discussed the possible role of ion production and loss mechanism and the O/N_2 ratio on the ionospheric delay against solar EUV flux. A strong effect of geomagnetic activity was reported. The ionosphere response time is controlled by photo-chemical, dynamical, and electrodynamic processes. The physical mechanisms of the time delay of daytime thermospheric temperature response has
85 been discussed by Ren et al. (2019). The time delay in the thermosphere temperature is due to the difference between the total heating and cooling rates. The study also found a possible role of the general circulations in the upper atmosphere on the time delay. Recently, Ren et al. (2020) discussed the physical mechanism using the TIE-GCM model to understand the physical mechanisms of the time delay in different thermospheric neutrals (O and N_2). They found that the the peak response time of neutral mass density corresponds to the time of equilibrium between the effect of the barometric process and the change in its
90 abundance.

Despite such a general understanding, however, the exact mechanism of the ionospheric delay needs further investigation. Therefore, here we attempt to quantify the process, which is probably responsible for the ionospheric delay by using the CTIpe model (Fuller-Rowell and Rees, 1980). Vaishnav et al. (2018) indicated that transport processes might be the primary cause for the delay observed in TEC using CTIpe model. Based on this assumption, numerical simulations have been performed to



95 consolidate the preliminary results of Vaishnav et al. (2018) and the hypothesis of Jakowski et al. (1991), and to explain the physical mechanisms of the ionospheric delay. To understand the role of T/I coupling in this study we perform model runs changing the eddy diffusion.

An ionospheric delayed response has been investigated by Schmölder et al. (2020) over European stations. They reported an ionospheric delay of about 18 h over these stations. Hence, in this paper, we emphasis to reproduce and investigate the
100 ionospheric delay response over an European location ($40^\circ N$).

2 CTIPe Model Simulations

The CTIPe model is used to understand the influence of eddy diffusion in the neutral composition, and its role in the delay mechanism. The CTIPe model is an advanced version of the CTIM model (Fuller-Rowell et al., 1987), and is a global, first principle, non-linear, time-dependent, 3-D, numerical, physics-based coupled thermosphere-ionosphere-plasmasphere model,
105 which consists of four fully coupled distinct components, namely (a) a neutral thermosphere model (Fuller-Rowell and Rees, 1980), (b) a high-latitude ionosphere convection model (Quegan et al., 1982), (c) a mid- and low-latitude ionosphere plasmasphere model (Millward et al., 1996), and (d) an electrodynamics model (Richmond et al., 1992). The thermosphere component of the CTIPe model solves the equations of continuity, momentum, and energy to calculate wind components, global temperature, and the composition.

110 The transport terms particularly specify the $E \times B$ drift and include ion-neutral interactions under the effect of the magnetospheric electric field. The geographic latitude/longitude resolution is $2^\circ/18^\circ$. In the vertical direction, the atmosphere is divided into 15 levels in logarithmic pressure at an interval of one scale height, starting from a lower boundary at 1 Pa (about 80 km altitude) to above 500 km altitude at pressure level 15. The high latitude ionosphere (poleward of geomagnetic coordinates $55^\circ N/S$) and the mid and low latitude ionosphere and plasmasphere are implemented as separate components and there
115 is an artificial boundary between these two model components. The equations for the neutral thermosphere model are solved self-consistently with a high-latitude ionospheric model (Quegan et al., 1982). The numerical solution of the composition equation describe transport, turbulence, and diffusion of atomic oxygen, molecular oxygen, and nitrogen (Fuller-Rowell and Rees, 1983). To run the model, external inputs are required like solar UV and EUV, Weimer electric field, TIROS/NOAA auroral precipitation (note, however, that particle precipitation is turned off during our simulations), and tidal forcing from the Whole
120 Atmosphere Model (WAM). The F10.7 index (Tapping, 1987) is used as input solar proxy to calculate ionization, heating, and oxygen dissociation processes. Within CTIPe, a reference solar spectrum based on the EUVAC model (Richards et al., 1994) and the Woods and Rottman (2002) model, driven by variations of input F10.7 is used. The EUVAC model is used for the wavelength range from 5 to 105 nm, and the Woods and Rottman (2002) model from 105 nm to 175 nm. Solar flux is obtained from the reference spectra using the following equation:

$$125 \quad f(\lambda) = f_{ref}(\lambda)[1 + A(\lambda)(P - 80)] \quad (1)$$



where f_{ref} and A are the reference spectrum and a solar variability factor, and $P = 0.5 \times (F10.7 + F10.7A)$, where $F10.7A$ is the average of $F10.7$ over 41 days. Detailed information on the CTIPE model is available in Codrescu et al. (2008, 2012).

In this paper, our primary goal is to understand the influence of eddy diffusion on the ionospheric reaction on the 27 days solar rotation. Therefore, in this study, different model runs were performed using different diffusion conditions with different artificial solar activity conditions. Three runs were performed with sinusoidally varying solar activity from 75-125 sfu, keeping all the other conditions constant. To perform these experiments, constant atmospheric and astronomical conditions of 15 March 2013 were used.

Several authors have suggested that the eddy diffusion is strongly varying based on the months or seasons (e.g., Kirchoff and Clemesha, 1983; Sasi and Vijayan, 2001; Swenson et al., 2019). Hence, the experiments were performed by using an eddy diffusion coefficient K_T , which amounts to 75%, 100%, and 125% of the original values in the model, and we refer to these runs as $K_T \times 0.75$, $K_T \times 1.0$, and $K_T \times 1.25$, with $K_T \times 1.0$ representing the reference run.

3 Mechanistic Studies

In the CTIPE model, the T/I composition is calculated by combining the continuity equation with the diffusion equation. The model estimates the changes in the composition of the major species (O , O_2 and N_2) self-consistently, including wind and temperature (Fuller-Rowell and Rees, 1983), as well as molecular diffusion, production, and loss mechanisms.

The continuity equation for the mass mixing ratio, $\psi_i = (n_i \cdot m_i) / \rho$ of the i -th species, with n_i as number density, m_i as the molecular mass, and ρ as atmospheric density, may be written as:

$$\frac{\partial \psi_i}{\partial t} = \frac{1}{\rho} (m_i S_i) - \mathbf{V} \cdot \nabla \psi_i - \omega \frac{\partial \psi_i}{\partial p} - \frac{1}{\rho} \nabla \cdot (n_i m_i \mathbf{C}_i) + \frac{1}{\rho} \nabla \cdot (K_T n \nabla m \psi_i), \quad (2)$$

where S_i represents sources and sinks of the species, K_T is the eddy diffusion coefficient, \mathbf{V} is the horizontal neutral wind vector, n is the total number density, m is the mean molecular mass and \mathbf{C}_i is the diffusion velocity of the i -th species. The terms on the right-hand side of equation (2) are, in their respective order, sources and sinks of species, horizontal advection, vertical advection, molecular diffusion, and eddy diffusion.

The mathematical form of the eddy diffusion coefficient K_T used in the CTIPE model as a function of height is given by Shimazaki (1971) and Fuller-Rowell and Rees (1992):

$$K_T = D \exp(-A_1(h - h_o)^2) \quad h \geq h_o, \quad (3)$$

$$K_T = (D - D_o) \exp(-A_2(h - h_o)^2) + D_o \exp(-A_3(h - h_o)) \quad h \leq h_o. \quad (4)$$

A peak value of $D = 150 \text{ m}^2 \text{ s}^{-1}$ at $h_o = 105 \text{ km}$ altitude and $D_o = 100 \text{ m}^2 \text{ s}^{-1}$ is used for the $K_T \times 1.0$ reference run. The shape parameters $A_1 = 0.03$, $A_2 = 0.03$, and $A_3 = 0.05$ are taken from Shimazaki (1971). As pointed out by Fuller-Rowell and



155 Rees (1992), eddy diffusion has the greatest effect on atomic oxygen and nitric oxide in the lower thermosphere. A detailed description of the chemistry of major species is available in Fuller-Rowell (1984).

In our experiments, the CTIPe model was first run for ten days with constant F10.7 input to reach a diurnally reproducible state, and after this spin-up, F10.7 was modified for 27 days using a sine function:

$$F10.7(t) = 100 - 25 \cos\left(\frac{2\pi t}{27}\right), \quad (5)$$

where t represents the time in days.

160 The different terms of the composition equation are shown in Figure 1 for the noontime (12 UT) for atomic oxygen mass mixing ratio (ψ_O) at $40^\circ N/18^\circ E$ in the reference run. The Figure shows the behavior of all terms at pressure level 12 (260 km). The vertical red dashed line shows the maximum of the input solar flux as per equation 2. Figure 1(a) shows that the molecular diffusion term shows a delay of less than one day for ψ_O . The horizontal and vertical advection are decreasing with the increasing input solar flux with a delay of less than one day and one day, respectively (Figure 1(b)). Similar variations can
 165 be seen in the chemical production and loss term (source and sink term). The delay between production and loss is about 1-2 days in the case of ψ_O as shown in Figure 1(c).

The change in the production term in the composition term based on the photoionization processes that contribute to ψ_O .

170 Ren et al. (2020) discussed the physics behind the time delay in different thermospheric neutrals. They found that the peak response time of neutral (O and N_2) mass density corresponds to the time of equilibrium between the effect of the barometric process and the change in its abundance.

Figure 2 shows the daily zonal mean TEC for three different runs with different eddy diffusion coefficients as a function of time and magnetic latitude. The zonal mean values represent the average TEC values over all longitudes at a specific magnetic latitude. In the CTIPe model, TEC is calculated from the altitude range of 80 km to 2000 km. In Figure 2, the zonal mean TEC is shown by the contours, and the white curves show the corresponding variability of the F10.7 index. Here, moderate solar

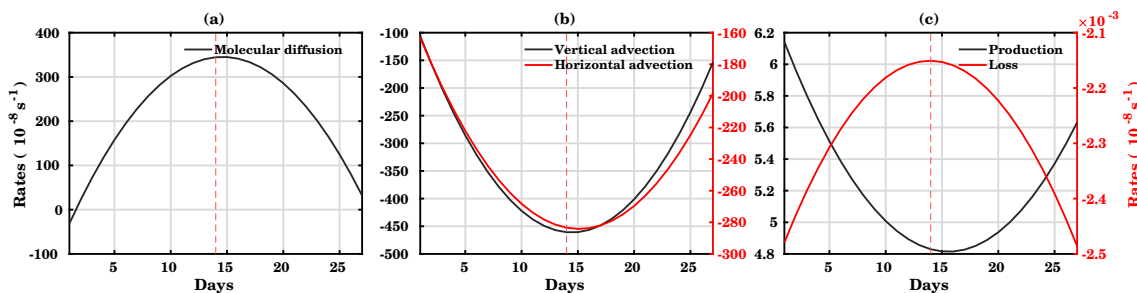


Figure 1. Time series of different terms: (a) molecular diffusion, (b) horizontal advection and vertical advection, and (c) production and loss for atomic oxygen mass mixing ratio. Both the y-axis marked with the corresponding color. The vertical red dashed line represents 14^{th} model day. All the parameters are plotted for pressure level 12 (260 km) for noontime at $40^\circ N/18^\circ E$.



175 activity conditions (75-125 sfu) have been used. The daily zonal mean TEC values indicate the overall effect of solar flux on
the T/I system, as for these simulations, we have used constant atmospheric and astronomical conditions.

The results from the reference run $K_T \times 1.0$, with the original value of the eddy diffusion coefficient, are shown in Figure
2(b). The simulations reproduce the real latitudinal as well as temporal variations with the variability in the solar flux. The
zonal mean TEC distributions are symmetric about the equator, with maximum amplitudes of about 70 TECU. The TEC
180 values decrease towards the high latitudes. The distribution of TEC highly depends on the ionization of neutrals and different
processes such as transport and recombination. The TEC amplitude variations reflect the effect of solar activity and composition
changes.

The $K_T \times 0.75$ run results are shown in Figure 2(a). It shows an increase of TEC in the low- to mid-latitude region in
comparison to reference run. The reduction of turbulence leads to slower transport and an increase in TEC. Figure 2(c) shows
185 zonal mean TEC for the $K_T \times 1.25$ run. In comparison to the reference run, TEC is decreased to a significant amount. These
results show that eddy diffusion has a direct effect on TEC.

Figure 3(a) shows the global mean TEC (GTEC) as simulated by the three different runs along with the F10.7 index (white
curve). It shows an obvious 27 days variation of GTEC according to the F10.7 index variations, but with a slightly different
delay for the different runs. The GTEC values are varying from about 8 TECU to reach maximum values of about 15 TECU
190 for the reference run according to solar flux variation. It can be seen that TEC increases linearly with F10.7. In comparison
to the reference run, TEC values decreased significantly for the increased eddy diffusion condition, while it is increased for
reduced eddy diffusion conditions (See also Figure 2).

The model input F10.7 index has been calculated according to Eq.(5), but as hourly values in order to calculate the delay
and the cross-correlation between GTEC and F10.7 shown in Figure 3(b).

195 For the reference run $K_T \times 1.0$, the delay is about 24 h, which is close to the value derived from observations as reported
by Schmöller et al. (2018, 2020). Hence, the model is capable of reproducing the observed ionospheric delay. In the case of
reduced eddy diffusion to 75% of the original value in run $K_T \times 0.75$, the delay is somewhat longer (about 25 h). This indicates
that the delay increases due to the slower transport processes in this run. In line with this, in the case of increased transport in

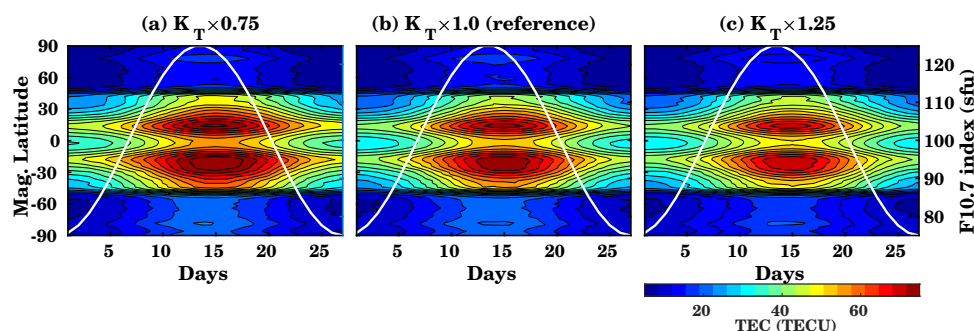


Figure 2. CTIPe simulated daily mean zonal mean TEC for the runs (a) $K_T \times 0.75$, (b) $K_T \times 1.0$ (reference), and (c) $K_T \times 1.25$. The white curves show the input F10.7 index.

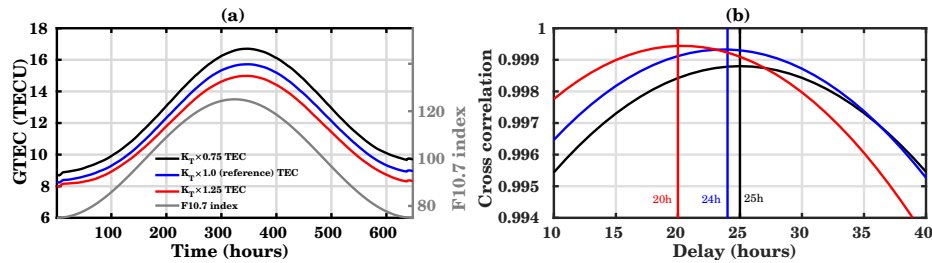


Figure 3. (a) Time series of modeled GTEC for different runs (a) $K_T \times 0.75$, (b) $K_T \times 1.0$ (reference), and (c) $K_T \times 1.25$, together with F10.7 given as a gray line. (b) Cross-correlation, and the delay between global mean TEC and F10.7 for the different runs.

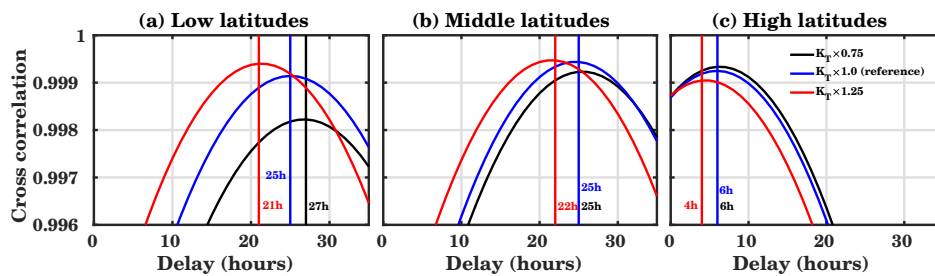


Figure 4. Cross-correlation and delay between regional mean TEC and the F10.7 index at low (a), middle (b), and high (c) geomagnetic latitudes for different runs.

run $K_T \times 1.25$, the delay is reduced to 20 h. These results suggest that an increase in the eddy diffusion leads to faster transport processes and an increased loss rate resulting in a decrease of the ionospheric time delay. The loss rates will be discussed below.

We have also analysed the model results for the Northern Hemisphere (NH) and the Southern Hemisphere (SH) separately, but the differences between hemispheres are small, and amount to 3 h, 4 h, and 4 h for the $K_T \times 0.75$, $K_T \times 1.0$, and $K_T \times 1.25$ runs, respectively (not shown).

Figure 4 shows the variation of the time delay at low [$\pm 30^\circ$], middle [$\pm(30^\circ - 60^\circ)$] and high [$\pm(60^\circ - 90^\circ)$] geomagnetic latitude regions for different eddy diffusion conditions. At low latitudes (Figure 4(a)), the delay is more sensitive to eddy diffusion than at middle and high latitudes, as this region is not only controlled by the EUV. Here dynamics plays an essential role, especially in the equatorial ionization anomaly. So small changes in the eddy diffusion may result in a more significant change of the ionospheric delay. Generally, at low latitudes, the delay is longer than for the global average in Figure 3. For the run $K_T \times 1.25$, the delay is reduced by 4 h as compared to the reference run.

At mid-latitudes (Figure 4(b)) the delay in the run $K_T \times 1.25$ is about 22 h, i.e. it is longer than on a global average. This is also true for the other runs where the delay is qualitatively the same and amounts to about 25 h. In this region for run $K_T \times 0.75$, the delay is similar to the one of the reference run and is about 25 h.

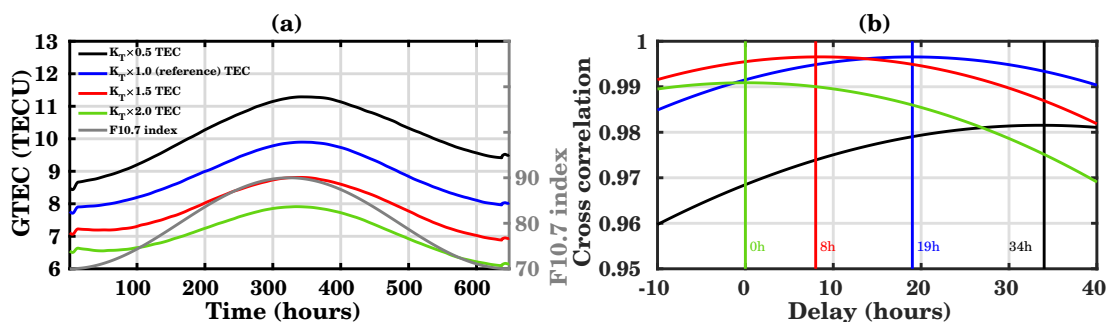


Figure 5. (a) Time series of modeled TEC for the different diffusion conditions $K_T \times 0.5$, $K_T \times 1.0$ (reference), $K_T \times 1.5$ and $K_T \times 2.0$. F10.7 is added as a gray line. (b) Cross-correlation, and the delay between global mean TEC and F10.7 for the different diffusion conditions.

At high latitudes (Figure 4(c)), the variation in the delay is qualitatively the same as at middle and low latitudes i.e., a decrease of diffusion increases the delay and vice versa. However, a change of diffusion has less effect at high latitudes, and the delay varies between 4 h and 6 h for the different runs. For all runs, at high latitudes, the delay is much smaller than at middle latitudes. In comparison to low and midlatitudes, the high latitudes show less time delay in run $K_T \times 0.75$. The delay at high latitudes is also less sensitive to diffusion changes as compared to the low and middle latitude regions.

Similar to the runs presented in Figure 3, the model has been run for low solar activity conditions with F10.7 ranging from 70-90 sfu, and using four different diffusion conditions $K_T \times 0.5$, $K_T \times 1.0$ (reference), $K_T \times 1.5$, and $K_T \times 2.0$, which amounts to 50%, 100%, 125% and 150% of the original values in the model, as shown in Figure 5. Figure 5(a) shows the time series of TEC for different runs and input F10.7. In comparison to Figure 3(a), the TEC values are smaller, following the F10.7 index. For these runs, the magnitude of eddy diffusion has been changed by 50%. Hence significant differences are observed in the TEC magnitude. In the reference run, TEC is varying from about 8 TEC to 11.3 TECU, while it shows a similar pattern for decreased/increased eddy diffusion with the difference in relative amplitude of TEC. The difference in the TEC curves in Figure 5(a) depends on the solar flux and the magnitude of the eddy diffusion coefficient. Furthermore, the delay is calculated by using the hourly TEC datasets and F10.7 index, as shown in Figure 3(a). For the reference run $K_T \times 1.0$, the delay in the simulated GTEC is about 19 h, while the delay is shifted to 34 h for the run $K_T \times 0.5$, and it decreases with the increased diffusion conditions. Here the delay is more sensitive to eddy diffusion compared to 25% change cases, as the solar activity is less dominant. In comparison to low solar activity, the eddy diffusion is less dominant under moderate solar activity, and the delay variations are reduced. It should be noted that the increasing solar activity leads to increase the ionospheric delay.

To shed more light on the spatial patterns of correlation between the F10.7 index and TEC and on the ionospheric delay, the latter is shown in Figure 6 at every model grid point. Figure 6(b) shows the spatial map for the reference run $K_T \times 1.0$. Maximum longitudinal differences are observed in the low and middle latitude region. Near the equatorial region, the delay is varying from 10 to 40 h. At high latitudes, the delay is about 0 to 10 h. The longitudinal variation of the delay follows the magnetic field. The maximum delay is, in line with the results in Figure 4, generally observed at lower and middle latitudes. As is the case with GTEC, at all latitudes, the delay in local TEC is generally increased in run $K_T \times 0.75$ and decreased in run

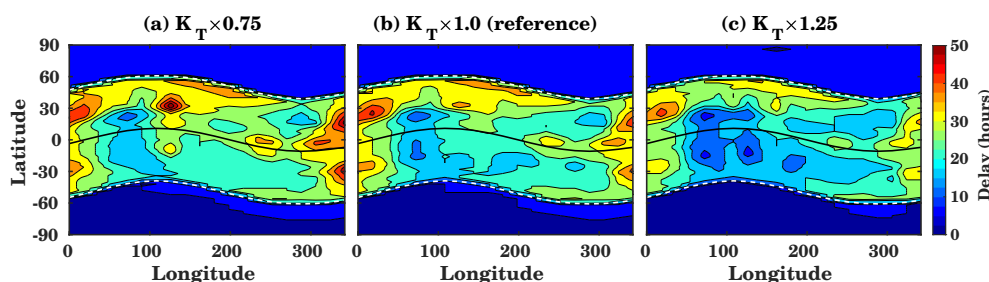


Figure 6. Spatial distribution of time delay between the CTIPe-TEC and the F10.7 index for different transport conditions (a) $K_T \times 0.75$, (b) $K_T \times 1.0$ (reference), and (c) $K_T \times 1.25$. The black line represents the magnetic equator, and dashed white lines represent magnetic latitudes 55° N/S).

$K_T \times 1.25$ with respect to run $K_T \times 1.0$. In the CTIPe model, the low and mid-latitude ionosphere model and high latitude ionosphere model are implemented separately. Hence the clear change in delay that can be seen at 55° N/S may be owing to model peculiarities in CTIPe.

In the following, we investigate the height variation of the delay using the atomic oxygen ion density at geographic coordinates $40^\circ N/18^\circ E$ (magnetic latitude $39.06^\circ N$). Figure 7 shows the delay between the atomic oxygen ion density and the F10.7 index at different pressure levels. At pressure level 12 (260 km), the delay is about 24h, 18h, and 6h for the different eddy diffusion cases $K_T \times 0.75$, $K_T \times 1.0$, and $K_T \times 1.25$, respectively. The delay further increases above pressure level 12, where it is quite close to the delay observed in TEC. This is owing to the fact that the delay observed in TEC is mainly determined by the delay of the F-region, i.e. at higher pressure levels (200-260 km).

To investigate how eddy diffusion influences the T/I system we further analyse the evolution of several thermospheric parameters such as atomic oxygen number density (n_O), molecular oxygen density (n_{O_2}), molecular nitrogen density (n_{N_2}), molecular oxygen dissociation rates (j_{O_2}), neutral temperature (T), and electron density (n_e). Figures 8 and 9 show variations of these parameters for the 27 days cycle for the reference run (blue color in the upper panel) and percentage differences (lower panel: on the second y-axis) from the reference run for the other diffusion conditions $K_T \times 0.75$ and $K_T \times 1.25$, respectively, at geographic coordinates $40^\circ N/18^\circ E$.

Figure 8 shows the variation in n_O , n_{N_2} , and n_{O_2} at pressure level 12 (~ 260 km). Eddy diffusion has a strong influence on O, N_2 , and O_2 . Figure 8(a) shows the atomic oxygen density variations at pressure level 12 for a 27 d solar rotation period. It shows that the atomic oxygen density decrease as solar radiation flux increases, connected with a temperature increase shown in Figure 9(a). In comparison to the reference run, the percentage difference increases to about 1% for the run $K_T \times 0.75$ during the 27 d run. This is partly, but not completely due to the temperature decrease by $\sim 0.7\%$ (Figure 9(a)). Thus, a decreased transport leads to reduced atomic oxygen. For the run $K_T \times 1.25$, atomic oxygen density decreases by about 1.5%. These differences are not connected with the solar cycle but evolve gradually over the full time interval.

Similar to the atomic oxygen density variations, the molecular oxygen and nitrogen densities also decrease with increasing solar flux (Figure 8(b) and 8(c)). For molecular oxygen density, the percentage difference decreases to about 10% for the run

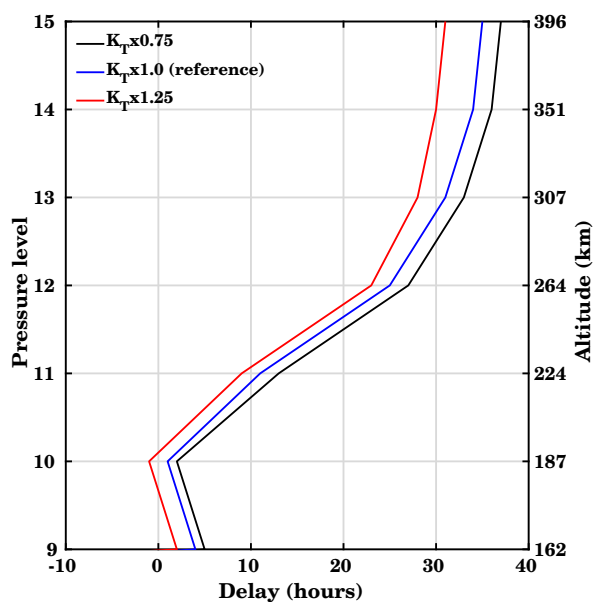


Figure 7. Vertical distribution of time delay between the atomic oxygen ion density and the F10.7 index for different transport conditions $K_T \times 0.75$, $K_T \times 1.0$ (reference), and $K_T \times 1.25$ at geographic coordinates $40^\circ N/18^\circ E$.

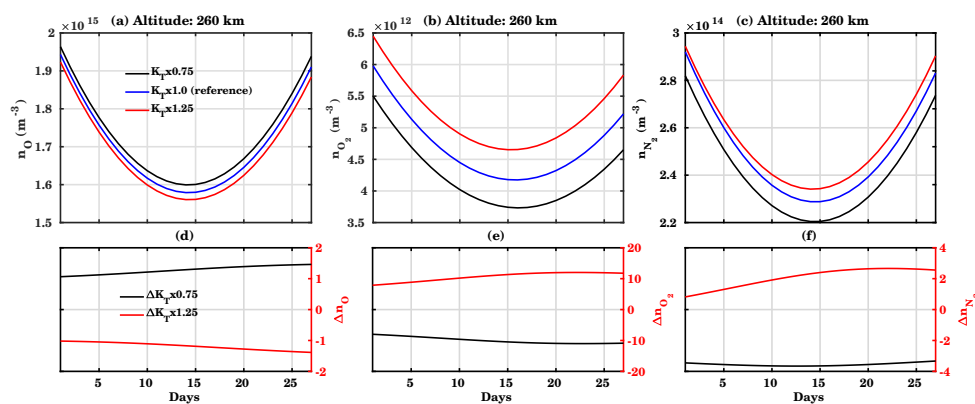


Figure 8. Variation of the CTIpe simulated (a) n_O , (b) n_{O_2} , and (c) n_{N_2} for different diffusion conditions $K_T \times 0.75$ (black), $K_T \times 1.0$ (blue) and $K_T \times 1.25$ (red) (upper panel) for the pressure level 12 (260 km). The percentage difference between the run $K_T \times 1.0$ (blue curve) and those with modified eddy diffusion conditions $K_T \times 0.75$ (black), and $K_T \times 1.25$ (red) are shown in the lower parts of the panels.



$K_T \times 0.75$, while it increases to about 10% for the $K_T \times 1.25$ run. Similar variations are observed in the molecular nitrogen density behaviour (Figure 8(c)). Once the diffusion increased, the n_{O_2} increases compared to the reference run, demonstrating that diffusion is a critical process to control the evolution of oxygen. Hence, we register an overall composition change due to an increase or decrease eddy diffusion.

Figure 8(d) and 8(b) shows the percentage difference between the reference run results and those of the runs with increased or decreased eddy diffusion. For the run $K_T \times 0.75$ the atomic oxygen density increases to about 1% whereas molecular oxygen decreases by 10%. Similar to molecular oxygen, molecular nitrogen density also decreases by $\sim 3\%$. In comparison to $K_T \times 0.75$, opposite trends can be seen for the run $K_T \times 1.25$.

In Figure 9(a) and 9(b), the 27 d behaviour at an altitude of ~ 260 km is shown for T and n_e . T increases with increasing solar radiation. As an increase in solar radiation will expand the thermosphere region, the scale height of each component is changing. An increase in the solar radiation flux will also increase the height of each pressure level. In Figure 9(e) non-monotonic variations are observed in the difference between the reference run and $K_T \times 1.25$. This might be due to the combined effect of different diffusion cases and solar flux. In comparison to the reference case, the temperature decreases by about 0.7% in the case of the $K_T \times 0.75$ run, while it increases by 0.7% for the $K_T \times 1.25$ run. Similar to T , n_e also varies with solar flux. An increase in the solar radiation flux leads to an increase in ionization and results in an increase of the electron density.

The j_{O_2} also vary for different diffusion conditions, as shown in Figure 9(c) for pressure level 7 (altitude ~ 125 km). An increase in the eddy diffusion reduces j_{O_2} , which results in increasing n_{O_2} , and a reduction in the n_O . Exactly the opposite behaviour is observed for a decrease of the eddy diffusion.

As we are dealing with the vertical transport processes, it is essential to analyze the latitudinal variation against pressure levels. Figure 10 shows the percentage difference of T , j_{O_2} , and n_e in runs $K_T \times 0.75$, and $K_T \times 1.25$ with respect to $K_T \times 1.0$ for the 14th model day. Figure 10(b) and 10(c) show that due to a reduction/increase of eddy diffusion, T decreases/increases at all pressure levels.

The lowest four pressure levels belong to the lower boundary, where the neutral wind, temperature, and height of the pressure level are imposed as a boundary conditions from the WAM model. An increase of the eddy diffusion by a factor of 25% ($K_T \times 1.25$) leads to an increase in T by 1%. It mainly influences the pressure levels 7-9 (125-160 km). The percentage difference in the T is negligible at pressure levels 5-6 (110 km), but variations increase with altitude. Figure 10(d), shows the latitude-pressure distribution of n_e . For the run $K_T \times 0.75$, it shows that for a reduction in eddy diffusion, n_e is increased in the thermosphere above pressure level 9 (160 km). Interestingly, above this altitude, n_e increases by about 7%. Electron density increases in the low latitude region at pressure level 4 (98 km) and in the high latitude region at pressure level 5 (105 km). The response of the thermosphere n_e to an enhancement of eddy diffusion is entirely different. For the run $K_T \times 1.25$, n_e decreases at higher altitudes, but it increases at the lower pressure levels except for mid-latitude at 98 km and high latitudes at 105 km.

The variation in j_{O_2} is shown in Figure 10(g). The percentage difference for the run $K_T \times 0.75$ in comparison to the reference run is decreased at pressure levels 5-7 (105-125 km) by about 7%, and it decreases for the run $K_T \times 1.25$ by 7%.

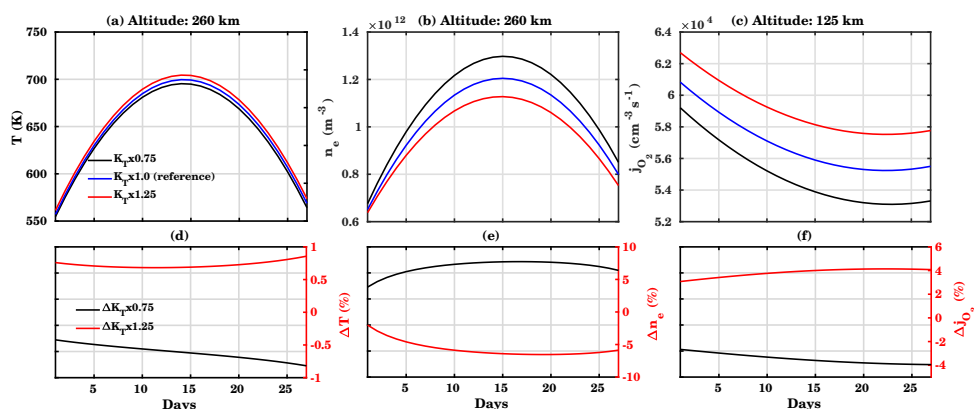


Figure 9. Same as Figure 8 for (a) T , (b) n_e for the pressure level 12 (~ 260 km), and (c) j_{O_2} for pressure level 7 (~ 125 km).

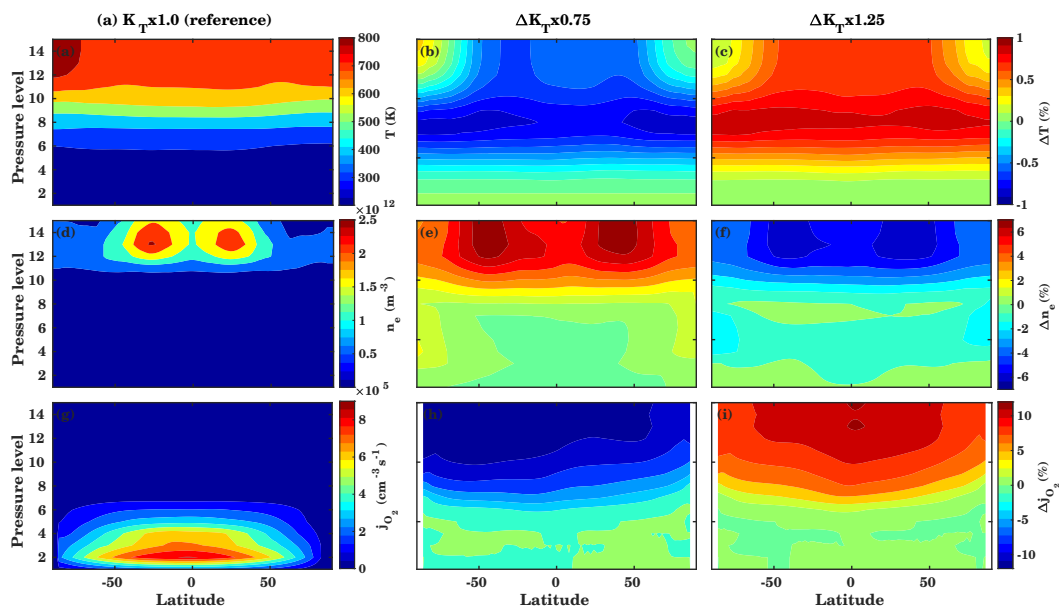


Figure 10. (a) CTIpe simulated T (upper row), n_e (middle row), and j_{O_2} (bottom row), for the 14th model day. The other columns show the percentage difference between the $K_T \times 1.0$ simulation and those with modified eddy diffusion conditions: (b) $K_T \times 0.75$ and (c) $K_T \times 1.25$.



Figure 11(a) shows the variation of n_O . For the run $K_T \times 0.75$, n_O is increased by 5-7% above the turbopause. Enhanced diffusion results in increased n_O in the lower thermosphere due to the downward transport of n_O from higher altitudes (Rees and Fuller-Rowell, 1988). Note that eddy diffusion has a more substantial impact at high latitudes below the turbopause. Chandra and Sinha (1974) showed that due to photochemical effects, the variation of eddy diffusion does not contribute significantly to n_O below 100 km, but above 100 km, it decreases with increasing eddy diffusion.

Enhanced eddy diffusion results in an enhancement of n_{O_2} of about 10-12% above the turbopause in the $K_T \times 1.25$ run, where j_{O_2} decreases by about 0.5%, as shown in Figure 10(d). So, the decrease in j_{O_2} increases n_{O_2} , and this results in a decrease of n_O .

Similar variations are also observed in the case of enhanced diffusion conditions for n_{N_2} with an increase of about 2-3% for the enhanced eddy diffusion conditions. The variation of the eddy diffusion affects the composition at different altitudes through molecular diffusion.

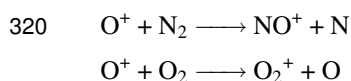
Enhanced eddy diffusion leads to an increase in molecular oxygen. This will lead to reduced atomic oxygen at all altitudes above 100 km through molecular diffusion. As a result, there is a significant reduction in the $[O]/[N_2]$ ratio. Qian et al. (2009) studied the effect of modified eddy diffusion on the thermospheric composition using the NCAR TIE-GCM model and reported similar results. These simulations revealed a new finding how eddy diffusion could strongly affect the thermospheric composition (O , O_2 , and N_2) through the ionospheric delay.

The steady-state electron density N can be written according to Rishbeth (1998):

$$N \sim \frac{q}{\beta} \sim \frac{I[O]}{\gamma_1[N_2] + \gamma_2[O_2]} \quad (6)$$

where q , β , I , and γ_1 , γ_2 are the production term, the loss term, solar ionizing flux and the reaction rates, respectively.

The composition of the T/I system is mainly controlled by various production and loss mechanisms. The production of electrons is mainly due to ionization of atomic oxygen through solar EUV, and loss is mainly controlled by N_2 . The production of atomic oxygen ions is not only depending on the atomic oxygen density, but also on solar radiation. Ren et al. (2018) explained that the delay observed in the electron density depends on the production and loss processes, as well as the $[O]/[N_2]$ ratio. The major loss of ions in the F regions is given by the following reactions:



The rate coefficients γ_1 and γ_2 in Eq.(6) are given, e.g., by St.-Maurice and Torr (1978). These reaction rate coefficients are dependent on the effective temperature (T_f), which significantly affects the loss reaction and composition:

$$T_f = 0.63 \times T_i + 0.36 \times T_N. \quad (7)$$

Here T_i and T_N are ion temperature and neutral temperature. For low values of $T_f < 1100K$, the loss rate coefficients γ_1 and γ_2 decrease with increasing T_f , while for $T_f > 1100K$, the loss rate γ_1 increases as a result of the electron density decrease with increasing F10.7 index. The nonlinear relation between the loss rate coefficients and T_f is shown by Su et al. (1999).



Figure 12 shows the variations of the $[O]/[N_2]$ ratio for different diffusion conditions at geographic lat/lon $40^\circ N/18^\circ E$ at an altitude of about 230 km (pressure level 12). For the reference run, the delay is about 2-3 days as the peak response is observed at day 16. The $[O]/[N_2]$ ratio strongly decreases with increasing eddy diffusion, and also the delay is shifted to one day. Hence the variation in eddy diffusion is strongly affecting the $[O]/[N_2]$ ratio, which further influences the delay mechanism.

Figure 13 shows the effect of eddy diffusion on the atomic oxygen ionization (a) and loss rates (c) through molecular nitrogen at $40^\circ N/18^\circ E$ and the difference between the reference run and other diffusion cases are shown in Figure 13(b) and 13(d). The reference case $K_T \times 1.0$, and the runs $K_T \times 0.75$, and $K_T \times 1.25$ are shown by blue, black, and red curves. The maximum ionization occurs at pressure level 9-10 (162-187 km) (Figure 13(a)). Figure 13(b) shows a decrease of ionization rates with enhanced eddy diffusion, whereas they are increased for reduced eddy diffusion. The production term in Eq.(6) strongly depends on the ionization rates and atomic oxygen density. Hence enhanced eddy diffusion decreases ionization and atomic oxygen density. Figure 13(d) shows that the loss rates are decreased by about 0.5 % in the F region in the case of enhanced eddy diffusion. Su et al. (1999) discussed the dependence of loss rates on the temperature. They suggested that the loss rate coefficient decreases with increasing T_f . Enhanced eddy diffusion leads to an increase in the molecular components while reducing atomic oxygen.

Hence, enhanced N_2 increases the overall loss term in Eq.(6) and reduces the electron density, and this results in a reduced delay in TEC. Based on the model simulations, we conclude that eddy diffusion is one of the major factors responsible for the changes in thermospheric composition and a major driver of the ionospheric delay. Although current investigation suggests that a small change in loss rates may affect delay for several hours, further numerical modeling is required using real observations and varying atmospheric conditions to understand the physical processes.

4 Summary

Using a 1-D model, Jakowski et al. (1991) first reported that the delay introduced in the ionosphere concerning solar EUV variations is probably due to the slow diffusion of atomic oxygen. Based on their hypothesis, the ionospheric delay in TEC simulated by the CTIPE model is consistent with the observations. Using the F10.7 index, the ionospheric delay at the solar rotation period is well reproduced and amounts to about 1 d (Jacobi et al., 2016; Schmölter et al., 2018). The thermosphere/ionosphere coupling plays an important role in the delay mechanism and this was reported in several studies, but it was barely investigated. Hence, this is the first time we investigated the impact of eddy diffusion on the ionospheric delay. To investigate the physical mechanism of the ionospheric delay at the solar rotation period, we have performed various experiments using the CTIPE model. From the mechanistic studies using CTIPE, results show that the eddy diffusion is the primary factor that strongly influences the delay introduced in the TEC based on the solar activity conditions. In the case of reduced eddy diffusion to 75% of the original value, the delay is somewhat longer (about 25 h), whereas in the case of increased transport, the delay is reduced to 20 h. An increase in the eddy diffusion leads to faster transport processes and an increased loss rates resulting in a decrease of the ionospheric time delay. At low latitudes, the influence of solar activity is stronger, as EUV radiation drives ionization

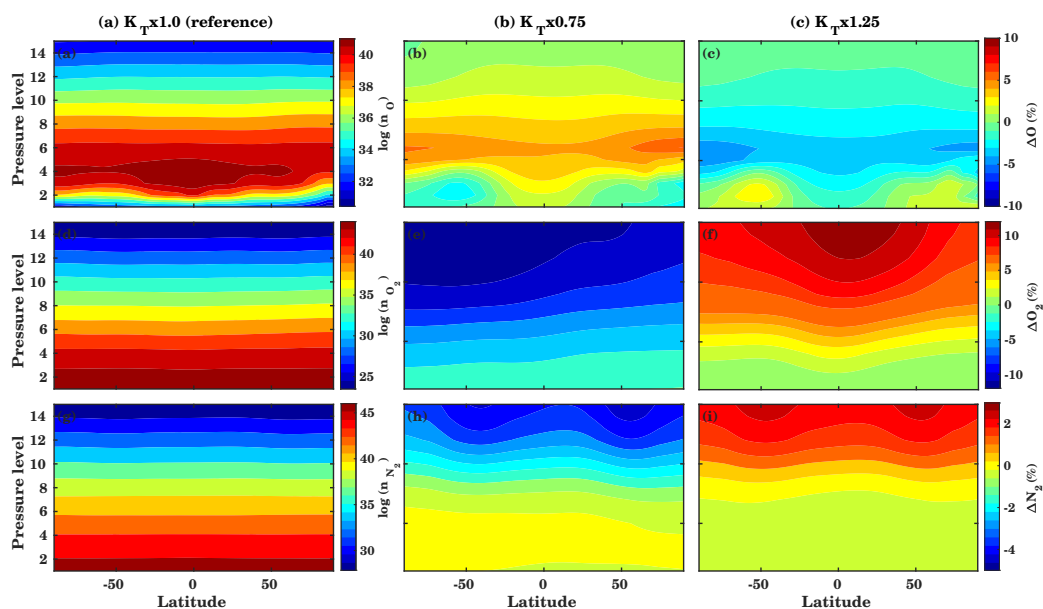


Figure 11. Same as Figure 10, but, for n_O , n_{O_2} , and n_{N_2} .

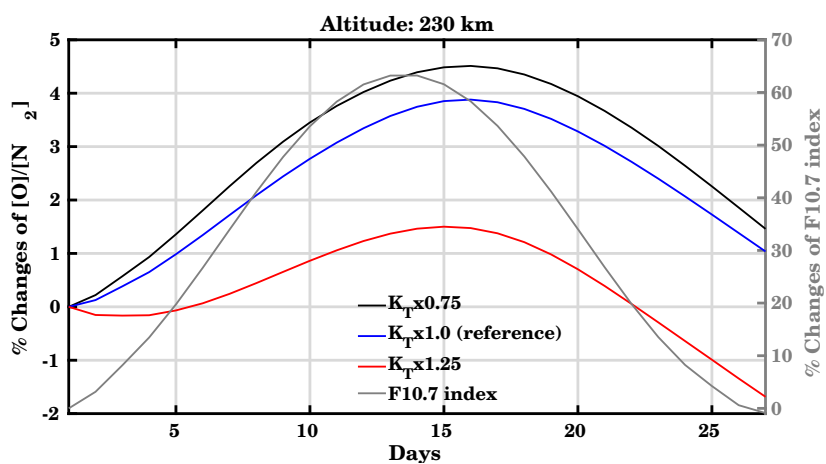


Figure 12. Percentage change of $[O]/[N_2]$ ratio for different diffusion conditions $K_T \times 0.75$, $K_T \times 1.0$ (reference), and $K_T \times 1.25$ at pressure level 12 at geographic coordinates $40^\circ N/18^\circ E$. The right y-axis refers to the percentage change of the F10.7 index (gray curve).

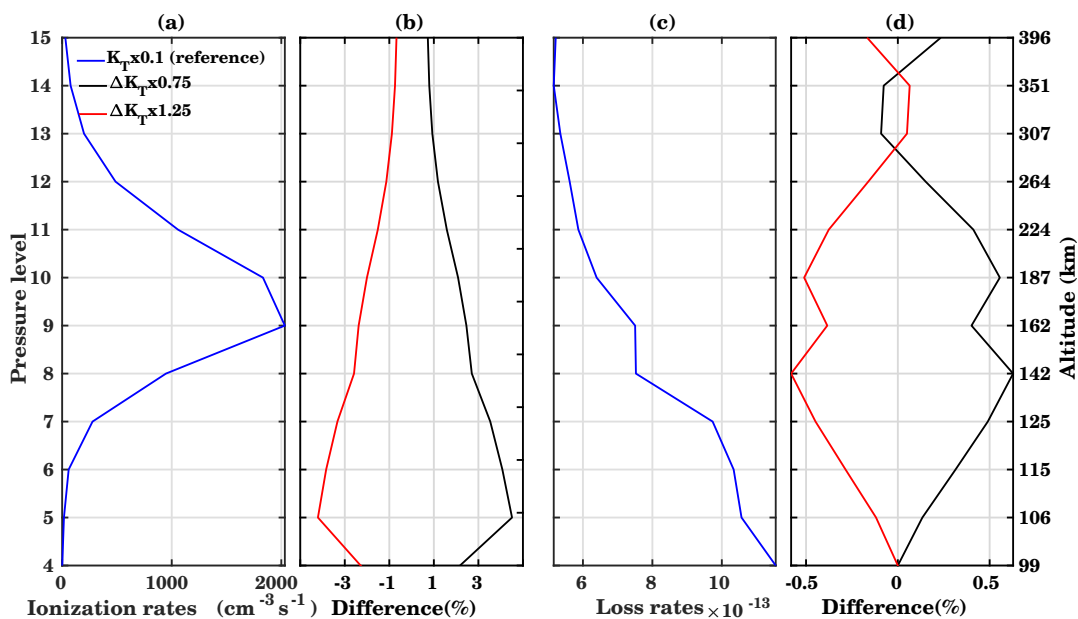


Figure 13. Atomic oxygen ionization (a) and loss rates (c) due to molecular nitrogen for the reference run $K_T \times 1.0$ and its difference (b,d) with $K_T \times 0.75$ and $K_T \times 1.25$ at different pressure levels on the 14th model day at geographic coordinates 40°N/18°E.

360 processes that lead to composition changes. Hence, the combined effect of eddy diffusion and solar activity shows more delay in the low and mid-latitude region.

Our results suggests that eddy diffusion plays a crucial role in the ionospheric delay. Hence, further numerical modeling and observational results are required to understand the in-depth role of lower atmospheric forcing and thermosphere/ionosphere coupling.

365 For this study, constant atmospheric conditions have been used to understand the role of solar flux and eddy diffusion in the ionospheric delay. In future, further investigation is required to explore the physical processes using actual observations. It would also be interesting to investigate the combined effect of solar variations, geomagnetic variations, and lower atmospheric forcing.

Author contributions. RV together with CJ and MC performed the CTIPe model simulations. RV drafted the first version of the manuscript.

370 All authors discussed the results and contributed to the final version of the manuscript.

Competing interests. Christoph Jacobi is one of the Editors-in-Chief of Annales Geophysicae. The authors declare that they have no conflict of interest.



Acknowledgements. The study has been supported by Deutsche Forschungsgemeinschaft (DFG) through grants No. BE 5789/2-1 and JA 836/33-1.



375 References

- Afraimovich, E. L., Astafyeva, E. I., Oinats, A. V., Yasukevich, Y. V., and Zhivetiev, I. V.: Global electron content: a new conception to track solar activity, *Annales Geophysicae*, 26, 335–344, <https://doi.org/10.5194/angeo-26-335-2008>, 2008.
- Anderson, P. C. and Hawkins, J. M.: Topside ionospheric response to solar EUV variability, *Journal of Geophysical Research: Space Physics*, 121, 1518–1529, <https://doi.org/10.1002/2015ja021202>, 2016.
- 380 Appleton, E. V.: Two Anomalies in the Ionosphere, *Nature*, 157, 691–691, <https://doi.org/10.1038/157691a0>, 1946.
- Brasseur, G. P. and Solomon, S.: *Aeronomy of the middle atmosphere: Chemistry and physics of the stratosphere and mesosphere*, vol. 32, Springer Science & Business Media, 2006.
- Chandra, S. and Sinha, A. K.: The role of eddy turbulence in the development of self-consistent models of the lower and upper thermospheres, *Journal of Geophysical Research*, 79, 1916–1922, <https://doi.org/10.1029/ja079i013p01916>, 1974.
- 385 Codrescu, M. V., Fuller-Rowell, T. J., Munteanu, V., Minter, C. F., and Millward, G. H.: Validation of the Coupled Thermosphere Ionosphere Plasmasphere Electrodynamics model: CTIPE-Mass Spectrometer Incoherent Scatter temperature comparison, *Space Weather*, 6, <https://doi.org/10.1029/2007sw000364>, 2008.
- Codrescu, M. V., Negrea, C., Fedrizzi, M., Fuller-Rowell, T. J., Dobin, A., Jakowsky, N., Khalsa, H., Matsuo, T., and Maruyama, N.: A real-time run of the Coupled Thermosphere Ionosphere Plasmasphere Electrodynamics (CTIPE) model, *Space Weather*, 10, <https://doi.org/10.1029/2011sw000736>, 2012.
- 390 Colegrove, F. D., Hanson, W. B., and Johnson, F. S.: Eddy diffusion and oxygen transport in the lower thermosphere, *Journal of Geophysical Research*, 70, 4931–4941, <https://doi.org/10.1029/jz070i019p04931>, 1965.
- Danilov, A. D. and Konstantinova, A. V.: Reduction of the atomic oxygen content in the upper atmosphere, *Geomagnetism and Aeronomy*, 54, 224–229, <https://doi.org/10.1134/s0016793214020066>, 2014.
- 395 Fuller-Rowell, T. J.: A two-dimensional, high-resolution, nested-grid model of the thermosphere: 1. Neutral response to an electric field “spike”, *Journal of Geophysical Research*, 89, 2971, <https://doi.org/10.1029/ja089ia05p02971>, 1984.
- Fuller-Rowell, T. J. and Rees, D.: A Three-Dimensional Time-Dependent Global Model of the Thermosphere, *Journal of the Atmospheric Sciences*, 37, 2545–2567, [https://doi.org/10.1175/1520-0469\(1980\)037<2545:atdtdg>2.0.co;2](https://doi.org/10.1175/1520-0469(1980)037<2545:atdtdg>2.0.co;2), 1980.
- Fuller-Rowell, T. J. and Rees, D.: Derivation of a conservation equation for mean molecular weight for a two-constituent gas within a three-
400 dimensional, time-dependent model of the thermosphere, *Planetary and Space Science*, 31, 1209–1222, [https://doi.org/10.1016/0032-0633\(83\)90112-5](https://doi.org/10.1016/0032-0633(83)90112-5), 1983.
- Fuller-Rowell, T. J. and Rees, D.: Turbulent diffusion variability and implications for the upper thermosphere, *Advances in Space Research*, 12, 45–56, [https://doi.org/10.1016/0273-1177\(92\)90443-2](https://doi.org/10.1016/0273-1177(92)90443-2), 1992.
- Fuller-Rowell, T. J., Rees, D., Quegan, S., Moffett, R., and Bailey, G.: Interactions between neutral thermospheric composition and the polar ionosphere using a coupled ionosphere-thermosphere model, *Journal of Geophysical Research*, 92, 7744, <https://doi.org/10.1029/ja092ia07p07744>, 1987.
- 405 Jacobi, C., Jakowski, N., Schmidtke, G., and Woods, T. N.: Delayed response of the global total electron content to solar EUV variations, *Advances in Radio Science*, 14, 175–180, <https://doi.org/10.5194/ars-14-175-2016>, 2016.
- Jakowski, N., Fichtelmann, B., and Jungstand, A.: Solar activity control of ionospheric and thermospheric processes, *Journal of Atmospheric and Terrestrial Physics*, 53, 1125–1130, [https://doi.org/10.1016/0021-9169\(91\)90061-b](https://doi.org/10.1016/0021-9169(91)90061-b), 1991.
- 410



- Jones, M., Forbes, J. M., and Hagan, M. E.: Tidal-induced net transport effects on the oxygen distribution in the thermosphere, *Geophysical Research Letters*, 41, 5272–5279, <https://doi.org/10.1002/2014gl060698>, 2014a.
- Jones, M., Forbes, J. M., Hagan, M. E., and Maute, A.: Impacts of vertically propagating tides on the mean state of the ionosphere-thermosphere system, *Journal of Geophysical Research: Space Physics*, 119, 2197–2213, <https://doi.org/10.1002/2013ja019744>, 2014b.
- 415 Jones, M., Emmert, J. T., Drob, D. P., Picone, J. M., and Meier, R. R.: Origins of the Thermosphere-Ionosphere Semiannual Oscillation: Reformulating the “Thermospheric Spoon” Mechanism, *Journal of Geophysical Research: Space Physics*, 123, 931–954, <https://doi.org/10.1002/2017ja024861>, 2018.
- Keneshea, T. J. and Zimmerman, S. P.: The Effect of Mixing Upon Atomic and Molecular Oxygen in the 70–170 km Region of the Atmosphere, *Journal of the Atmospheric Sciences*, 27, 831–840, [https://doi.org/10.1175/1520-0469\(1970\)027<0831:teomua>2.0.co;2](https://doi.org/10.1175/1520-0469(1970)027<0831:teomua>2.0.co;2), 1970.
- 420 Kirchoff, V. W. J. H. and Clemesha, B. R.: Eddy diffusion coefficients in the lower thermosphere, *Journal of Geophysical Research*, 88, 5765, <https://doi.org/10.1029/ja088ia07p05765>, 1983.
- Lee, C.-K., Han, S.-C., Bilitza, D., and Seo, K.-W.: Global characteristics of the correlation and time lag between solar and ionospheric parameters in the 27-day period, *Journal of Atmospheric and Solar-Terrestrial Physics*, 77, 219–224, <https://doi.org/10.1016/j.jastp.2012.01.010>, 2012.
- 425 Li, F., Liu, A. Z., and Swenson, G. R.: Characteristics of instabilities in the mesopause region over Maui, Hawaii, *Journal of Geophysical Research*, 110, <https://doi.org/10.1029/2004jd005097>, 2005.
- Liu, L., Wan, W., Ning, B., Pirog, O. M., and Kurkin, V. I.: Solar activity variations of the ionospheric peak electron density, *Journal of Geophysical Research*, 111, <https://doi.org/10.1029/2006ja011598>, 2006.
- Meraner, K. and Schmidt, H.: Transport of nitrogen oxides through the winter mesopause in HAMMONIA, *Journal of Geophysical Research: Atmospheres*, 121, 2556–2570, <https://doi.org/10.1002/2015jd024136>, 2016.
- 430 Millward, G., Moffett, R., Quegan, S., and Fuller-Rowell, T.: A coupled thermosphere-ionosphere-plasmasphere model (CTIP), STEP handbook on ionospheric models, pp. 239–279, 1996.
- Pilinski, M. D. and Crowley, G.: Seasonal variability in global eddy diffusion and the effect on neutral density, *Journal of Geophysical Research: Space Physics*, 120, 3097–3117, <https://doi.org/10.1002/2015ja021084>, 2015.
- 435 Qian, L., Solomon, S. C., and Kane, T. J.: Seasonal variation of thermospheric density and composition, *Journal of Geophysical Research: Space Physics*, 114, <https://doi.org/10.1029/2008ja013643>, 2009.
- Qian, L., Burns, A. G., Solomon, S. C., and Wang, W.: Annual/semiannual variation of the ionosphere, *Geophysical Research Letters*, 40, 1928–1933, <https://doi.org/10.1002/grl.50448>, 2013.
- 440 Quegan, S., Bailey, G., Moffett, R., Heelis, R., Fuller-Rowell, T., Rees, D., and Spiro, R.: A theoretical study of the distribution of ionization in the high-latitude ionosphere and the plasmasphere: first results on the mid-latitude trough and the light-ion trough, *Journal of Atmospheric and Terrestrial Physics*, 44, 619–640, [https://doi.org/10.1016/0021-9169\(82\)90073-3](https://doi.org/10.1016/0021-9169(82)90073-3), 1982.
- Rees, D. and Fuller-Rowell, T.: Understanding the transport of atomic oxygen within the thermosphere, using a numerical global thermospheric model, *Planetary and Space Science*, 36, 935–948, [https://doi.org/10.1016/0032-0633\(88\)90101-8](https://doi.org/10.1016/0032-0633(88)90101-8), 1988.
- 445 Ren, D., Lei, J., Wang, W., Burns, A., Luan, X., and Dou, X.: Does the Peak Response of the Ionospheric F2 Region Plasma Lag the Peak of 27-Day Solar Flux Variation by Multiple Days?, *Journal of Geophysical Research: Space Physics*, 123, 7906–7916, <https://doi.org/10.1029/2018ja025835>, 2018.



- Ren, D., Lei, J., Wang, W., Burns, A., Luan, X., and Dou, X.: A Simulation Study on the Time Delay of Daytime Thermospheric Temperature Response to the 27-Day Solar EUV Flux Variation, *Journal of Geophysical Research: Space Physics*, 124, 9184–9193, <https://doi.org/10.1029/2019ja027000>, 2019.
- 450 Ren, D., Lei, J., Wang, W., Burns, A., Luan, X., and Dou, X.: Different Peak Response Time of Daytime Thermospheric Neutral Species to the 27-Day Solar EUV Flux Variations, *Journal of Geophysical Research: Space Physics*, 125, <https://doi.org/10.1029/2020ja027840>, 2020.
- Richards, P. G., Fennelly, J. A., and Torr, D. G.: EUVAC: A solar EUV Flux Model for aeronomic calculations, *Journal of Geophysical Research*, 99, 8981, <https://doi.org/10.1029/94ja00518>, 1994.
- 455 Richmond, A. D., Ridley, E. C., and Roble, R. G.: A thermosphere/ionosphere general circulation model with coupled electrodynamic, *Geophysical Research Letters*, 19, 601–604, <https://doi.org/10.1029/92gl00401>, 1992.
- Rishbeth, H.: How the thermospheric circulation affects the ionospheric F2 layer, *Journal of Atmospheric and Solar-Terrestrial Physics*, 60, 1385–1402, [https://doi.org/10.1016/s1364-6826\(98\)00062-5](https://doi.org/10.1016/s1364-6826(98)00062-5), 1998.
- Rishbeth, H., Fuller-Rowell, T., and Rees, D.: Diffusive equilibrium and vertical motion in the thermosphere during a severe magnetic storm : A computational study, *Planetary and Space Science*, 35, 1157–1165, [https://doi.org/10.1016/0032-0633\(87\)90022-5](https://doi.org/10.1016/0032-0633(87)90022-5), 1987.
- 460 Sasi, M. N. and Vijayan, L.: Turbulence characteristics in the tropical mesosphere as obtained by MST radar at Gadanki (13.5°N, 79.2°E), *Annales Geophysicae*, 19, 1019–1025, <https://doi.org/10.5194/angeo-19-1019-2001>, 2001.
- Schmölter, E., Berdermann, J., Jakowski, N., Jacobi, C., and Vaishnav, R.: Delayed response of the ionosphere to solar EUV variability, *Advances in Radio Science*, 16, 149–155, <https://doi.org/10.5194/ars-16-149-2018>, 2018.
- 465 Schmölter, E., Berdermann, J., Jakowski, N., and Jacobi, C.: Spatial and seasonal effects on the delayed ionospheric response to solar EUV changes, *Annales Geophysicae*, 38, 149–162, <https://doi.org/10.5194/angeo-38-149-2020>, 2020.
- Shim, J. S., Kuznetsova, M., Rastätter, L., Hesse, M., Bilitza, D., Butala, M., Codrescu, M., Emery, B., Foster, B., Fuller-Rowell, T., Huba, J., Mannucci, A. J., Pi, X., Ridley, A., Scherliess, L., Schunk, R. W., Stephens, P., Thompson, D. C., Zhu, L., Anderson, D., Chau, J. L., Sojka, J. J., and Rideout, B.: CEDAR Electrodynamic Thermosphere Ionosphere (ETI) Challenge for systematic as-
470 sessment of ionosphere/thermosphere models: NmF2, hmF2, and vertical drift using ground-based observations, *Space Weather*, 9, <https://doi.org/10.1029/2011sw000727>, 2011.
- Shimazaki, T.: Effective eddy diffusion coefficient and atmospheric composition in the lower thermosphere, *Journal of Atmospheric and Terrestrial Physics*, 33, 1383–1401, [https://doi.org/10.1016/0021-9169\(71\)90011-0](https://doi.org/10.1016/0021-9169(71)90011-0), 1971.
- Siskind, D. E., Drob, D. P., Dymond, K. F., and McCormack, J. P.: Simulations of the effects of vertical transport on the
475 thermosphere and ionosphere using two coupled models, *Journal of Geophysical Research: Space Physics*, 119, 1172–1185, <https://doi.org/10.1002/2013ja019116>, 2014.
- St.-Maurice, J. P. and Torr, D. G.: Nonthermal rate coefficients in the ionosphere: The reactions of O⁺ with N₂, O₂, and NO, *Journal of Geophysical Research*, 83, 969, <https://doi.org/10.1029/ja083ia03p00969>, 1978.
- Su, Y. Z., Bailey, G. J., and Fukao, S.: Altitude dependencies in the solar activity variations of the ionospheric electron density, *Journal of*
480 *Geophysical Research: Space Physics*, 104, 14 879–14 891, <https://doi.org/10.1029/1999ja900093>, 1999.
- Swenson, G., Yee, Y., Vargas, F., and Liu, A.: Vertical diffusion transport of atomic oxygen in the mesopause region consistent with chemical losses and continuity: Global mean and inter-annual variability, *Journal of Atmospheric and Solar-Terrestrial Physics*, 178, 47–57, <https://doi.org/10.1016/j.jastp.2018.05.014>, 2018.



- 485 Swenson, G. R., Salinas, C. C. J. H., Vargas, F., Zhu, Y., Kaufmann, M., Jones, M., Drob, D. P., Liu, A., Yue, J., and Yee, J. H.: Determination of Global Mean Eddy Diffusive Transport in the Mesosphere and Lower Thermosphere From Atomic Oxygen and Carbon Dioxide Climatologies, *Journal of Geophysical Research: Atmospheres*, 124, 13 519–13 533, <https://doi.org/10.1029/2019jd031329>, 2019.
- Tapping, K. F.: Recent solar radio astronomy at centimeter wavelengths: The temporal variability of the 10.7-cm flux, *Journal of Geophysical Research*, 92, 829, <https://doi.org/10.1029/jd092id01p00829>, 1987.
- 490 Vaishnav, R., Jacobi, C., Berdermann, J., Schmölter, E., and Codrescu, M.: Ionospheric response to solar EUV variations: Preliminary results, *Advances in Radio Science*, 16, 157–165, <https://doi.org/10.5194/ars-16-157-2018>, 2018.
- Vaishnav, R., Jacobi, C., and Berdermann, J.: Long-term trends in the ionospheric response to solar extreme-ultraviolet variations, *Annales Geophysicae*, 37, 1141–1159, <https://doi.org/10.5194/angeo-37-1141-2019>, 2019.
- Woods, T. N. and Rottman, G. J.: Solar ultraviolet variability over time periods of aeronomic interest, in: *Atmospheres in the Solar System: Comparative Aeronomy*, pp. 221–233, American Geophysical Union, <https://doi.org/10.1029/130gm14>, 2002.